Enhancing the corrosion resistance of Cu/Ni-P/Au electrical contacts by electropolymerized poly(methyl methacrylate)

Ahmad Bahramian, Marielle Eyraud, Sébastien Maria, F. Vacandio, T. Djenizian, P. Knauth

Enhancing the corrosion resistance of Cu/Ni-P/Au electrical contacts by electropolymerized poly(methyl methacrylate)

A. Bahramian[a], M. Eyraud[a]*, S. Maria[b], F. Vacandio[a], T. Djenizian[c], P. Knauth[a]

[a] Aix Marseille Univ, CNRS, Madirel, UMR 7246, Electrochemistry of Materials Group, Campus St Jérôme, 13397 Marseille, France

[b] Aix Marseille Univ, CNRS, Institut de Chimie Radicalaire, UMR 7273, Campus St Jérôme, 13397 Marseille, France

[c] Mines Saint-Etienne, Center of Microelectronics in Provence, Department of Flexible Electronics, 13541 Gardanne, France

* Corresponding author: marielle.eyraud@univ-amu.fr

Highlights

- Modifying electrical contacts by electropolymerization of MMA is studied.
- Ten times increase in the corrosion resistance of electrical contacts is observed.
- The electrical resistance increased, but remained well below the accepted limit.
- Cathodic electrodeposition of PMMA effectively sealed the pores of Au top-layer.

Abstract

Cu/Ni-P/Au multi-layer systems are employed as electrical contacts. The Au top-layer is thin and porous. These pores deliver the corrosive media to the under-layer, which induces the corrosion by a galvanic coupling mechanism. Therefore, filling these pores is essential to improve the lifetime of electronic devices. The pores can be sealed by the electrodeposition of poly(methyl methacrylate) that decreased the porosity index (about 97%) and increased the corrosion resistance (about 10 times) of electrical contacts after 10 cycles of electropolymerization. A non-uniform polymeric film, however, was formed at higher number of polymerization cycles (> 50) that decreased the corrosion resistance.

1. Introduction

Electrical contacts allow exchanging information between a reader and an embedded chip. They are extensively applicable in relays, contactors, switches, and circuit breakers [1,2]. An electrical contact usually consists of a multilayer Cu/Ni/Au thin film stacked to an epoxy tape. Cu is used due to its high electrical conductivity but this metal highly suffers from a poor corrosion resistance and oxidation resistance that increase its resistivity. Au acts as a protective layer against corrosion. However, Cu rapidly diffuses through Au and thus even a thick layer of Au cannot protect it. Therefore, Ni or Ni-P are utilized as a diffusion barrier layer. The incorporation of

P changes the crystalline structure of Ni deposits to an amorphous state. Therefore, Ni-P films have superior properties due to the lack of crystalline defects (such as grain boundaries) that serve as preferential sites for diffusion of chemical species and localized reactions like corrosion. The required thickness of Au is reported to be drastically reduced when amorphous Ni-P films are used. The Au film is notably thin due to its high cost; the total thickness of the Ni barrier layer and Au film remains below 3 μm [3,4].

However, the porosity of thin films increases with decreasing the thickness. Hence, thin top Au films in electrical contacts are to some extent porous [4]. The pores act as channels and deliver corrosive media to the under-layer [2]. The galvanic coupling inside these pores is responsible for the fast corrosion of the Ni barrier layer based on the well-known "small anode surface (Ni) – large cathode surface (Au)" phenomenon. After dissolution of Ni films, the subsequent attack of the Cu substrate occurs [3]. Note that corrosion products are often electrical insulators, they can terminate the functionality of electrical contacts [5]. Therefore, improving the corrosion resistance of electrical contacts extends their lifetime and thus has economic and ecological benefits [6]. It is, however, a huge challenge, since Cu, Ni, and Au have a large difference in their standard potentials and any modification should not increase the electrical resistance above a low acceptable value [2].

Self-assembled monolayers (SAMs) have shown promising results in improving the corrosion behavior of metals [7–9]. These organic molecules are adsorbed on the surface and form ordered domains. The interaction between SAMs and the substrate can be more or less intensive, depending if the molecules possess a head group with a strong affinity that anchors the molecule to the substrate. SAMs can then modify the porosity of thin films and thus improve the corrosion resistance [2,6,10]. In the case of the Cu/Ni/Au multilayer system, if these molecules accumulate at the pores of the substrate, they can limit the accessibility of the barrier layer to the corrosive media [11]. Song et al. [6] successfully decreased the porosity index of an Au top-coat using SAMs (AUTRONEX™ Nano 104S). However, the application of SAMs may increase the electrical resistivity [12]; furthermore, it suffers from bad reproducibility and is not cost-effective [13].

Employing polymers is a well-known strategy to enhance the corrosion resistance [14–17]. Surface anomalies and irregularities, such as pores or surface roughness, have a different surface energy and thus they can act as polymerization centers [18,19]. It was found that pores have a strong free-energy minimum. The monomer,

therefore, can be adsorbed (partially or completely) inside the pore and polymerize there [20]. As a result, it is theoretically possible to fill the pores of thin Au with polymers. However, most organic coatings suffer from a poor adhesion to their metallic substrate. Poly(methyl methacrylate) or PMMA can be strongly chemisorbed (electrografted) on metals owing to its carbonyl functionality [21,22]. PMMA is a transparent colorless polymer with a low molecular weight showing high corrosion and chemical resistance [23]. Interestingly, it is possible to etch PMMA using UV [24–26] for removing polymer grown outside the pores that partially covers the gold surface and thus enhances the electrical resistivity. As a result, PMMA seems to be a potential candidate to improve the corrosion behavior of electrical contacts.

Electropolymerization is a simple and economical technique that initiates and terminates the chemical reaction through the transfer of electrons [27]. The cathodic electropolymerization of MMA can then be employed to avoid the oxidation of the metallic electrode during the process [22]. Note that this process has been already used to fill titania nanotubes with PMMA for energy storage applications [28–32]. An adequate solvent for electropolymerization should be able to dissolve the monomer and support salt in order to provide sufficient conductivity. In this context, dimethyl sulfoxide (DMSO) is reported to be an excellent solvent for MMA [27].

In this study, the effects of cathodic electropolymerization of MMA (methyl methacrylate) from DMSO on the corrosion behavior of Cu/Ni-P/Au electrical contacts is investigated for the first time. Several techniques including Scanning Electron Microscopy (SEM), Grazing Angle X-Ray Diffraction (Grazing XRD), Electrochemical Impedance Spectroscopy (EIS), Cyclic Polarization (CP), and Salt Spray (SS) tests were implemented to characterize Cu/Ni-P/Au electrical contacts before and after modification with PMMA.

2. Experimental procedure

A DMSO based solution containing 0.1 M KNO_3 (as supporting electrolyte) and 4 vol.% MMA was used to electropolymerize MMA on samples. KNO_3 was added to DMSO and the solution then was stirred for 60 minutes. MMA was added to the solution and the stirring continued for another 30 minutes. Highly pure chemicals (provided by Sigma-Aldrich) were used as received.

A potentiostat/galvanostat (BioLogic VP300) was employed to perform all electrochemical tests in a three-electrode setup containing the sample as the working electrode, a Pt plate as the counter electrode, and an Ag/AgCl (KCl saturated) reference electrode. Cyclic voltammetry (CV) was used in a cathodic window (-0.5 to -2.0 V) with a scan rate of 20 mV.s^{-1} to polymerize MMA at room temperature. Different cycle numbers, 5, 10, 15, 25, 50, and 100 cycles, were used to modify Cu/Ni-P/Au electrical contacts provided by our industrial partner. The metallic multilayer systems have a total thickness of about 35 μm and are deposited on an epoxy support. The samples were named after their corresponding cycle number, e.g. C0 represents the unmodified sample and C25 is the sample modified by 25 cycles of MMA polymerization. All the samples were washed with distilled water and dried with compressed air after the process.

A precision scale ($\pm 10^{-4}$ g) was used to determine the mass of polymer by subtracting the mass before polymerization from the mass after polymerization. The electrical resistivity of samples was measured by a precise Ohm meter (± 1 mΩ) using the classical four-probe measurement.

The surface morphology and chemical composition of the samples were investigated by a scanning electron microscope (model Philips XL 30 ESEM) equipped with an Energy Dispersive Spectroscopy (EDS) analyzer. The EDS tests were done at 22 keV accelerating voltage. A CARL ZEISS/Ultra 55 scanning electron microscope was employed for the cross-section images. The crystalline structure of the samples was evaluated using a Siemens D5000 diffractometer. Cu Kα radiation ($\lambda = 0.15406$ nm) generated at 40 kV and 30 mA was used to obtain XRD patterns with 0.04° step size over a 2θ range of 25–70°.

The corrosion behavior of the samples was investigated by Electrochemical Impedance Spectroscopy (EIS) and Cyclic Polarization (CP) tests. The samples were immersed in a 3% NaCl solution for 60 minutes. The EIS measurements were carried out at Open Circuit Potential (OCP) from 100 kHz to 10 mHz (frequency range) with 10 mV voltage amplitude (peak-to-peak). The obtained EIS data were analyzed using Zview software. The CP experiments were done at a scan rate of 0.5 mV/s from -300 mV (vs. OCP) to 500 mV (vs. reference electrode) as the vertex point and reversed at 0 mV (vs. reference) as the finishing point. All the tests were repeated three times and the results were normalized by the exposed area to the corrosive media.

An Ascott S450 Salt Spray apparatus was employed to do SS tests. The SS tests were carried out in accordance with the B 117 ASTM standard. The surface of the samples was periodically evaluated during the SS test by an optical microscope (ARISTOMET) at 100x magnification. The obtained images were analyzed by ImageJ software.

3. Results and Discussion

- Electropolymerization

Figure 1 presents the CV curves of MMA electropolymerization on the samples in a potential range between -0.5 to -2.0 V vs. Ag/AgCl. The inlay in that figure corresponds to a smaller potential range (-0.5 to -1.5 V). The first cycle (in blue) clearly presents two reductions waves: the first one between -1.2 to -1.8 V where the reduction current is followed by a plateau, the second one below -1.8 V leading to a steep rise in current.

The increase in the number of cycles, till 25 cycles, induces a rapid decrease of the cathodic current in the both regions I and II (see the inlay, for the region I). This decrease is a direct evidence of electropolymerization: the global amount of polymer grafted during each scan is reduced because of the blocking of cathodic sites by the polymer during the previous scans. This result is in good accordance with pervious works [33–35]. Another way to interpret this current decrease is that the amount of polymer at the surface increases during each cycle of polymerization increasing the electrode resistance [33,34]. Interestingly, after 50 cycles a reverse trend was observed: the cathodic current started again to increase and its value after 100 cycles was even slightly higher than after 10 cycles. The formation of a thick mechanically unstable PMMA layer can lead to the detachment from the electrode and thus exposes the metallic surface [33].

Baute *et al.* [22] investigated the cathodic electropolymerization mechanism of some acrylate monomers (including MMA) form dimethylformamide (DMF). CV curves of the investigated acrylic monomers had 2 cathodic peaks. The first peak at less negative potentials was ascribed to the passivation of surface due to the adsorption of reduced monomer. The second peak was attributed to diffusion control. The first peak (around -1.8 V) was considered the critical potential at which the reaction of electrografting happens. Note that the partial electrografting of MMA occurs even before the first peak. This is in agreement with our results where

5

electropolymerization was carried out from -0.5 to -1.5 V (see inlay in Figure 1) and a similar decrease in current was observed.

The effect of electropolymerization cycles on the mass gain of samples is illustrated in Figure 2. A strong increase of sample mass can be seen in the first 5 cycles, followed by a slow mass increase between C5 to C50 with a quasi-constant slow rate of deposition. This result is in good accordance with the small variation of the current on CV curves in Figure 1 between C5 to C25. Then a drastic mass increase is observed after 50 cycles. This could be simply due to the higher polymerization amount at higher polymerization cycles or to a non-uniform polymerization.

- Chemical characterizations

The EDS technique was employed to assess the amount of C (and thus the polymer amount) as a function of the electropolymerization cycle number (Figure 2). The C content increases rapidly till C5 and then almost linearly between 5 to 100 cycles. The chemical composition of C0 was 3.3 wt.% Cu, 80.6 wt.% Ni, 5.7 wt.% P, and 10.4 wt.% Au. The EDS analysis was done at the center of each sample where a uniform distribution of current is expected. Therefore, the inconsistency between the increase of C content and mass gained after 50 cycles could be due to the non-uniform polymerization of MMA especially at the sample edges.

No polymer should be formed in the absence of a current flow [33]. To prove that, a sample was immersed in the electrolyte for 4 hours (that is the equivalent time of 100 cycles of electropolymerization). No supplementary amount of C was found, showing that PMMA was formed due to the applied potential.

To test the solubility of the formed PMMA in relation to the interaction between the polymer and the surface, C10 and C100 were immersed in tetrahydrofuran (THF) for 12 hours. The C amounts were 4.8 and 10.3 % for C10 and C100, respectively, so quite similar to the first analysis (4.2 and 9.2 % respectively). The insolubility of the formed PMMA in THF suggests a strong chemical grafting between Au and the electrodeposited polymer [33].

Figure 3 shows the grazing-incidence XRD patterns of C0 and C100. The observed peaks for C0 are related to Au, Ni, and Cu substrate. The strong Cu peak can be justified (200 main orientation) by the low thickness (and the partly amorphous nature) of the Ni-P barrier layer and Au top-coat, and also the porosity of the Au film. The XRD pattern intensity is related to the X-ray penetration depth [36], but

pores can intensify the penetration of X-rays [37]. The C100 pattern was almost similar to C0. However, it showed an increase of the intensity at low diffraction angles and a notable decrease in the intensity of the peaks attributed to Cu and Ni. Note that the intensity for Au is almost intact. The formation of an amorphous phase, here PMMA, on the surface of metals increases the X-ray intensity at low diffraction angles [38–40]. The intensity decrease of Cu and Ni can be attributed to the PMMA-filled pores.

- Morphological characterizations

Figure 4 shows optical microscopy images of C0. The micrometer-sized pores are obviously distributed all over the surface. SEM observations of the surface morphology of C0 and C100 are presented in Figure 5 (a and b). Both samples present a similar morphology except that C100 is slightly blurred, possibly due to the presence of a PMMA insulating deposit. At lower magnification, however, C100 has two distinct features (noted α and β in Figure 5c).

Figure 5c-e shows a non-uniform formation of polymer on the surface. This non-uniformity of PMMA has been previously reported even at higher concentrations of monomer [33]. The bright objects (marked as α) were found for all PMMA modified samples. The bright objects in SE mode are dark spots in the BSE mode, which is sensitive to the chemical composition (i.e. average atomic number) contrast [41] (Figure 5d). This means they are composed of a material with a low atomic number. Figure 5e shows one of these objects with a low electron beam power (to have a better resolution). Point EDS on this object showed 47.7 wt.% C that proves it is in fact made of PMMA. This object could have been formed in (on) the pores due to the similarities between the black spots in Figure 5d and pores in Figure 4a.

The halo shapes (marked as β in Figure 5c) were observed only for C50 and C100. A point EDS analysis showed 16.3 wt.% C (about 7 % higher than the overall C content of C100) that suggests a localized polymerization. All the pores could be filled after a certain number of cycles. The polymerization continues on any available surface since preferential sites (such as pores) are not available, leading to the formation of halo shapes in C50 and C100.

The cross-section of C100 is shown in Figure 5f. The polymeric features are obvious on the surface of samples. Therefore, PMMA covered the surface and sealed the

pores. The Au layer with about 100 nm thickness on about 1.5 μm thick Ni-P can be also seen in this figure.

- Electrical resistivity study

The electrical resistance of samples as a function of the electropolymerization cycle is depicted in Figure 2. C100 showed a 91% increase in the electrical resistivity. However, its resistance (40.7 mΩ) is still much lower than the resistivity limit of electrical contacts (300 mΩ) [42]. PMMA, therefore, is a potential candidate to enhance the lifetime of electrical contacts. Moreover, Figure 2 supports the presence of a non-uniform polymer layer because a strong resistivity increase should be observed in the presence of a uniform polymeric film [43–45].

- Corrosion resistance study

Figure 6 shows the EIS results obtained for samples with (C5-C100) and without (C0) the presence of PMMA. C0 and C5-C100 had asymmetric and symmetric Bode phase curves (Figure 6b), respectively. This suggests that while C0 has two time-constants, the PMMA modified samples present only one-time constant. The value of Z at low frequencies in the Bode modulus plots (Figure 6c) represents the corrosion resistance of samples. The highest corrosion resistance was observed for 10 cycles of MMA electropolymerization. This maximum can be also observed in the Nyquist plots, where it corresponds to the maximum diameter of the semi-circles (Figure 6a).

The equivalent circuits are represented in Figure 7. Rs is the solution resistance, which has a constant value of 5-6 Ωcm^2 for all experiments. Constant Phase Elements (CPE) are used to represent the non-ideal capacitive behavior of the samples. The CPE impedance is defined as:

$$Z_{CPE} = \frac{1}{Y_0(i\omega)^n} \qquad (1)$$

Y_0 is the constant of admittance, i is the imaginary unit, ω (= $2\pi f$) is the angular frequency, and n is the CPE exponent [46]. The n factor is sometimes known as the roughness factor since it is often affected by the surface roughness [47]. The polymer area grows after each cycle of polymerization that should lead to a rougher surface. The values of n can therefore be used to determine the effect of the polymerization

8

on the surface roughness. Increasing the roughness decreases the value of n ($n=1$ corresponds to an ideal parallel-plate capacitance) in agreement with our experimental data, where n gradually decreased from 0.93 (C0) to 0.83 (C100).

In the equivalent circuits, we assume that the initial sample shows pores where corrosion can occur. The fast dissolution of Ni in the pores occurs due to the galvanic coupling between Au (cathode) and Ni (anode). The value of n for CPE_p is 0.52 suggesting that the corrosion process inside the pores is under mass transport control [48,49]. CPE_{dl} and R_{ct} represent the double layer capacitance and the charge transfer resistance of the electrode, respectively. The CPE_{dl} shows typical values for a metallic electrode ($n \approx 1$ and Q in the μF cm^{-2} range). In the PMMA-modified samples, the pores are filled with the polymer, limiting the corrosion. The proposed equivalent circuits perfectly fitted the experimental data. The fitted values (analyzed by ZVIEW) are summarized in Table 1 and Table 2.

Assuming that the pores are filled with PMMA after polymerization, the elements representing the pores are substituted with CPE_{Pol} and R_{Pol} that are related to the capacitance and resistance behavior of the polymer. The equivalent circuit in Figure 7b explains the corrosion behavior of the modified samples. This model, however, can be simplified to a Randles model where:

$$CPE_t = CPE_{dl} + CPE_{Pol} \qquad\qquad (2)$$

And

$$R_t = \frac{R_{ct} \times R_{Pol}}{R_{ct} + R_{Pol}} \qquad\qquad (3)$$

While the metallic surface area decreases during the polymerization, the polymer surface area increases. Therefore, R_{ct} decreases after each cycle, while R_{Pol} increases.

Pores are confined spaces and an intensified corrosion process occurs inside them. Filling pores blocks these highly active corrosion sites and thus improves the overall corrosion resistance [50]. Increasing the cycle number of polymerization, however, decreases the uniformity of the surface. Therefore, the corrosion resistance decreases, because a non-uniform protective layer actually promotes the corrosion by leaving a limited exposed area in the corrosive media [51].

9

Figure 8 shows the CP curves of C0, C10, C100, and the Ni-P barrier layer. A pseudo-passivation behavior in the anodic branch of the Ni-P barrier was observed, as it was previously reported [52]. C0 showed the same behavior.

The Tafel extrapolation method was used to obtain the corrosion current density (i_{corr}), the corrosion potential (E_{corr}), and the anodic (β_a) and cathodic (β_c) slopes from CP tests. These data are used to calculate the polarization resistance (R_P) by the Stern-Geary equation [53]. The corresponding data are summarized in Table 3.

$$R_P = \frac{\beta_a \beta_c}{2.303(\beta_a + \beta_c) i_{corr}} \tag{4}$$

The comparison of β_a for C0 and the Ni-P barrier layer (58 vs. 137 mV.dec^{-1}, respectively) suggests a fast anodic reaction for C0. This anodic reaction could be attributed to the fast dissolution of the Ni-P underlayer due to the galvanic corrosion occurring inside the pores. The passivation behavior was not observed for PMMA modified samples, possibly due to the filled pores.

Polarization resistance values were in good agreement with those obtained from EIS tests and C10 revealed the highest resistance value. PMMA-covered samples had a nobler corrosion potential than C0. The more positive corrosion potential can be interpreted as the reduction of the corrosion inclination [54]. Decreasing the porosity shifts the corrosion potential to less cathodic values and decreases the corrosion current density [55]. Therefore, PMMA modified samples should have a lower porosity content. The porosity index (P.I) of surface coatings can be estimated by inserting the corrosion potential difference between the coated sample and the substrate (ΔE), the substrate polarization resistance (R_{ps}), the substrate anodic slope (β_a), and the coating polarization resistance (R_p) Eq. 5 [56].

$$P.I = \frac{R_{ps}}{R_p} \times 10^{-(\frac{\Delta E}{\beta_a})} \tag{5}$$

P.I values for C0 and C10 were 0.0269 and 0.0008, respectively, showing a 97% decrease in the porosity of the Au top-layer after 10 cycles of electropolymerization of MMA. A positive hysteresis loop was observed for all samples indicating that the occurrence of localized corrosion is inevitable. Au is generally known to be chemically inert. However, it can be corroded under anodic polarization and in the presence of chloride or bromide ions (due to the formation of Au complexes) [57]. Moreover, random pits can be always formed on the surface of metals due to their autocatalytic nature [58]. The corrosion could be even more severe for Au thin films.

Figure 9 shows the surface of samples after CP tests. The surface of C0 was severely damaged and the Cu substrate can be easily seen. The corrosion on the PMMA modified samples was restricted to the formation of green spots, and C10 had the lowest number of spots. These green corrosion products are reported to be clinoatacamite ($Cu_2(OH)_3Cl$) [4]. Therefore, the amount of Cu, Cl, and O after corrosion tests can demonstrate the corrosion progress (Figure 10). According to this figure, C10 presents the lowest content of Cu, O, and Cl and therefore the highest corrosion resistance. The content trends of Cu, Cl, and O (as a function of the polymerization cycle) are in good agreement with the respective polarization resistance and charge transfer resistance values.

The salt spray test, which is one of the most employed techniques to determine the atmospheric corrosion behavior of materials, was used to evaluate C0 and C10 in a long-time exposure (10 days) to corrosive media. However, the mass loss (gain) was reported to be negligible for electrical contacts during the salt spray test. As a result, weight measurement is not a suitable technique to estimate the corrosion of electrical contacts [3]. The pit size was therefore traced and compared for C0 and C10 (Figure 11). C0 showed a fast increase in the pit size after 48 hours and large pits were obvious after 240 hours. On the other hand, C10 showed a slow growth of pit area with a surface morphology almost unchanged after 240 hours. However, new pits were formed pointing out that the pitting corrosion is inevitable. EIS was used to verify the long-term corrosion behavior of the samples. As it was mentioned above, the |Z| values at low frequencies (i.e. 10 mHz) can be used to determine the corrosion resistance. Figure 12 shows the Bode Z plots of C0 and C10 during 240 hours of immersion in 3% NaCl. While the corrosion resistance of C0 gradually decreased (from 80 to 12 $k\Omega.cm^2$), C10 presented a stable resistance value during 10 days.

In conclusion, all corrosion tests, including EIS and salt spray tests, showed that the corrosion resistance of electrical contacts can be significantly improved by depositing PMMA. The best results were obtained using 10 electropolymerization cycles of MMA monomer. The electropolymerization of MMA is a valuable post-treatment method to enhance the corrosion resistance of electrical contacts.

4. Conclusions

The corrosion behavior of Cu/Ni-P/Au electrical contacts can be effectively modified by cathodic electrodeposition of PMMA. A strongly electrografted PMMA is formed on top of the electrical contacts and thus seals the pores of the Au thin top-

layer. The polymerization preferentially starts at surface defects like pits and pores. Continuing the polymerization when there is no preferential site available leads to a non-uniform growth of PMMA. Therefore, a maximum of corrosion resistance as a function of polymerization cycles is expected (10 cycles in this study). A further increase of the number of polymerization cycles leads to the formation of a non-uniform polymeric film. The sealed pores disconnect the Ni-P barrier layer from the corrosive media and thus improve the corrosion resistance by eliminating the galvanic coupling between the Au top-coat (cathode) and the Ni-P under-layer (anode). The PMMA modified electrical contacts have a high stability against corrosion at high exposure times (10 days). Although PMMA slightly increases the sample resistance, the resistance values are notably lower than the accepted limit for electrical contacts. As a result, electrodeposition of PMMA is an economical solution to improve the lifetime of electrical contacts. Moreover, this technique could be applicable to compensate the negative effects of porosity in other systems as well. The fretting corrosion of electrical contacts, due to the lubricating nature of polymers, may also be improved; this point will be subject of further investigations.

References

[1] M. Uysal, H. Akbulut, M. Tokur, H. Algül, T. Çetinkaya, Structural and sliding wear properties of Ag/Graphene/WC hybrid nanocomposites produced by electroless co-deposition, Journal of Alloys and Compounds. 654 (2016) 185–195. doi:10.1016/j.jallcom.2015.08.264.

[2] Z.H. Huang, Y.J. Zhou, W. He, A combination of self-assembled monolayer and hydrophobic conformal coating for anti-corrosion of Cu/NiP/Au 3D circuitry in artificial sweat solution, Surface and Coatings Technology. 320 (2017) 126–131. doi:10.1016/j.surfcoat.2017.01.087.

[3] V.K. Murugan, Z. Jia, G.J. Syaranamual, C.L. Gan, Y. Huang, Z. Chen, An investigation into different nickel and nickel–phosphorus stacked thin coatings for the corrosion protection of electrical contacts, Surface and Coatings Technology. 300 (2016) 95–103. doi:10.1016/j.surfcoat.2016.05.013.

[4] V.K. Murugan, Z. Jia, G.J. Syaranamual, C.L. Gan, Y. Huang, Z. Chen, Atmospheric corrosion resistance of electroplated Ni/Ni–P/Au electronic contacts, Microelectronics Reliability. 60 (2016) 84–92. doi:10.1016/j.microrel.2016.02.014.

[5] K. Meyyappan, G. Murtagian, A. Kurella, B. Pathangey, A. McAllister, S. Parupalli, Corrosion Studies on Gold-Plated Electrical Contacts, IEEE Transactions on Device and Materials Reliability. 14 (2014) 869–877. doi:10.1109/TDMR.2014.2333758.

[6] J. Song, L. Wang, A. Zibart, C. Koch, Corrosion Protection of Electrically Conductive Surfaces, Metals. 2 (2012) 450–477. doi:10.3390/met2040450.

[7]   T. Shimura, K. Aramaki, Improvement of the film thickness by modification of the hydroxymethylbenzene SAM with tetraethoxysilane and octanediol for protection of iron from corrosion in 0.5M NaCl, Corrosion Science. 50 (2008) 1397–1405. doi:10.1016/j.corsci.2007.12.010.

[8]   A.-R. El-Sayed, U. Harm, K.-M. Mangold, W. Fürbeth, Protection of galvanized steel from corrosion in NaCl solution by coverage with phytic acid SAM modified with some cations and thiols, Corrosion Science. 55 (2012) 339–350. doi:10.1016/j.corsci.2011.10.036.

[9]   C. Li, L. Li, C. Wang, Y. Zhu, W. Zhang, Study of the protection performance of self-assembled monolayers on copper with the scanning electrochemical microscope, Corrosion Science. 80 (2014) 511–516. doi:10.1016/j.corsci.2013.12.003.

[10] S. Nineva, S. Berger, F. Talgner, U. Electroplating, New Post-Treatment Process with Enhanced Technical Performance: Corrosion Protection for Electrical Contacts, (n.d.).

[11] D.A. Patel, A.M. Weller, R.B. Chevalier, C.A. Karos, E.C. Landis, Ordering and defects in self-assembled monolayers on nanoporous gold, Applied Surface Science. 387 (2016) 503–512. doi:10.1016/j.apsusc.2016.05.149.

[12] M. Hakamada, N. Kato, M. Mabuchi, Electrical resistivity of nanoporous gold modified with thiol self-assembled monolayers, Applied Surface Science. 387 (2016) 1088–1092. doi:10.1016/j.apsusc.2016.07.059.

[13] D. Capitao, B. Limoges, C. Fave, B. Schöllhorn, On the decisive role of the sulfur-based anchoring group in the electro-assisted formation of self-assembled monolayers on gold, Electrochimica Acta. 257 (2017) 165–171. doi:10.1016/j.electacta.2017.09.163.

[14] A.M. Fenelon, C.B. Breslin, The electropolymerization of pyrrole at a CuNi electrode: corrosion protection properties, Corrosion Science. 45 (2003) 2837–2850. doi:10.1016/S0010-938X(03)00104-5.

[15] D. Kowalski, M. Ueda, T. Ohtsuka, The effect of ultrasonic irradiation during electropolymerization of polypyrrole on corrosion prevention of the coated steel, Corrosion Science. 50 (2008) 286–291. doi:10.1016/j.corsci.2007.05.027.

[16] Z. Grubač, I.Š. Rončević, M. Metikoš-Huković, Corrosion properties of the Mg alloy coated with polypyrrole films, Corrosion Science. 102 (2016) 310–316. doi:10.1016/j.corsci.2015.10.022.

[17] İ. Çakmakcı, B. Duran, M. Duran, G. Bereket, Experimental and theoretical studies on protective properties of poly(pyrrole-co-N-methyl pyrrole) coatings on copper in chloride media, Corrosion Science. 69 (2013) 252–261. doi:10.1016/j.corsci.2012.12.011.

[18] A. Baumgärtner, M. Muthukumar, Effects of surface roughness on adsorbed polymers, The Journal of Chemical Physics. 94 (1991) 4062–4070. doi:10.1063/1.460656.

[19] J.F. Douglas, How Does Surface Roughness Affect Polymer-Surface Interactions?, Macromolecules. 22 (1989) 3707–3716.

[20] G.F. Hermsen, N.F.A. van der Vegt, M. Wessling, Monte Carlo Calculations of Polymer Adsorption at the Entrance of Cylindrical Pores in Flat Adsorbing Surfaces, Soft Materials. 1 (2003) 295–312. doi:10.1081/SMTS-120026595.

[21] N. Baute, L. Martinot, R. Jérôme, Investigation of the cathodic electropolymerization of acrylonitrile, ethylacrylate and methylmethacrylate by coupled quartz crystal microbalance analysis and cyclic voltammetry, Journal of Electroanalytical Chemistry. 472 (1999) 83–90.

[22] S.L. Cram, G.M. Spinks, G.G. Wallace, H.R. Brown, Electrochemical polymerization of acrylics on stainless steel cathodes, Journal of Applied Polymer Science. 87 (2003) 765–773. doi:10.1002/app.11436.

[23] G. Lu, Y.-M. Li, C.-H. Lu, Z.-Z. Xu, Corrosion protection of iron surface modified by poly(methyl methacrylate) using surface-initiated atom transfer radical polymerization (SI-ATRP), Colloid and Polymer Science. 288 (2010) 1445–1455. doi:10.1007/s00396-010-2283-x.

[24] B. Braren, D. Seeger, Low temperature UV laser etching of PMMA: On the mechanism of ablative photodecomposition (APD), Journal of Polymer Science Part C: Polymer Letters. 24 (1986) 371–376. doi:10.1002/pol.1986.140240802.

[25] R.W. Johnstone, I.G. Foulds, M. Parameswaran, Deep-UV exposure of poly(methyl methacrylate) at 254 nm using low-pressure mercury vapor lamps, Journal of Vacuum Science & Technology B: Microelectronics and Nanometer Structures. 26 (2008) 682. doi:10.1116/1.2890688.

[26] N. Yufa, S. Fronk, S.B. Darling, R. Divan, W. Lopes, S.J. Sibener, Modifying metal–polymer nanostructures using UV exposure, Soft Matter. 5 (2009) 1683. doi:10.1039/b820775e.

[27] B.L. Funt, K.C. Yu, Electroinitiated polymerization of methyl methacrylate in a homogeneous medium, Journal of Polymer Science. 62 (1962) 359–367. doi:10.1002/pol.1962.1206217408.

[28] G.D. Salian, C. Lebouin, A. Demoulin, M.S. Lepihin, S. Maria, A.K. Galeyeva, A.P. Kurbatov, T. Djenizian, Electrodeposition of polymer electrolyte in nanostructured electrodes for enhanced electrochemical performance of thin-film Li-ion microbatteries, Journal of Power Sources. 340 (2017) 242–246. doi:10.1016/j.jpowsour.2016.11.078.

[29] N. Plylahan, S. Maria, T.N. Phan, M. Letiche, H. Martinez, C. Courrèges, P. Knauth, T. Djenizian, Enhanced electrochemical performance of Lithium-ion batteries by conformal coating of polymer electrolyte, Nanoscale Research Letters. 9 (2014) 544. doi:10.1186/1556-276X-9-544.

[30] N.A. Kyeremateng, F. Dumur, P. Knauth, B. Pecquenard, T. Djenizian, Electrodeposited copolymer electrolyte into nanostructured titania electrodes for 3D Li-ion microbatteries, Comptes Rendus Chimie. 16 (2013) 80–88. doi:10.1016/j.crci.2012.05.002.

[31] N. Plylahan, N.A. Kyeremateng, M. Eyraud, F. Dumur, H. Martinez, L. Santinacci, P. Knauth, T. Djenizian, Highly conformal electrodeposition of copolymer electrolytes into titania nanotubes for 3D Li-ion batteries, Nanoscale Research Letters. 7 (2012) 349. doi:10.1186/1556-276X-7-349.

[32] N.A. Kyeremateng, F. Dumur, P. Knauth, B. Pecquenard, T. Djenizian, Electropolymerization of copolymer electrolyte into titania nanotube electrodes for high-performance 3D microbatteries, Electrochemistry Communications. 13 (2011) 894–897. doi:10.1016/j.elecom.2011.03.026.

[33] S. Cram, Mechanism of electropolymerisation of methyl methacrylate and glycidyl acrylate on stainless steel, Electrochimica Acta. 47 (2002) 1935–1948. doi:10.1016/S0013-4686(02)00097-X.

[34] M. Braglia, I.V. Ferrari, L. Pasquini, T. Djenizian, M. Sette, M.L. Di Vona, P. Knauth, Electrochemical synthesis of thin, dense, and conformal anion exchange membranes with quaternary ammonium groups, Electrochimica Acta. 265 (2018) 78–88. doi:10.1016/j.electacta.2018.01.151.

[35] I.V. Ferrari, M. Braglia, T. Djenizian, P. Knauth, M.L. Di Vona, Electrochemically engineered single Li-ion conducting solid polymer electrolyte on titania nanotubes for microbatteries, Journal of Power Sources. 353 (2017) 95–103. doi:10.1016/j.jpowsour.2017.03.141.

[36] G. Sundararajan, L. Rama Krishna, Mechanisms underlying the formation of thick alumina coatings through the MAO coating technology, Surface and Coatings Technology. 167 (2003) 269–277. doi:10.1016/S0257-8972(02)00918-0.

[37] J.A. Curran, T.W. Clyne, Porosity in plasma electrolytic oxide coatings, Acta Materialia. 54 (2006) 1985–1993. doi:10.1016/j.actamat.2005.12.029.

[38] T. Weisemoeller, F. Bertram, S. Gevers, C. Deiter, A. Greuling, J. Wollschläger, Effect of amorphous interface layers on crystalline thin-film x-ray diffraction, Physical Review B. 79 (2009). doi:10.1103/PhysRevB.79.245422.

[39] S.E. Fritz, S.M. Martin, C.D. Frisbie, M.D. Ward, M.F. Toney, Structural Characterization of a Pentacene Monolayer on an Amorphous SiO_2 Substrate with Grazing Incidence X-ray Diffraction, Journal of the American Chemical Society. 126 (2004) 4084–4085. doi:10.1021/ja049726b.

[40] H. Sirringhaus, P.J. Brown, R.H. Friend, M.M. Nielsen, K. Bechgaard, B.M.W. Langeveld-Voss, A.J.H. Spiering, R.A.J. Janssen, E.W. Meijer, P. Herwig, Two-dimensional charge transport in self-organized, high-mobility conjugated polymers, 401 (1999) 4.

[41] L. Reimer, Imaging with Secondary and Backscattered Electrons, in: Scanning Electron Microscopy, Springer, Berlin, Heidelberg, 1985: pp. 227–271. doi:10.1007/978-3-662-13562-4_6.

[42] J. Song, C. Koch, L. Wang, Correlation between Wear Resistance and Lifetime of Electrical Contacts, Advances in Tribology. 2012 (2012) 1–9. doi:10.1155/2012/893145.

[43] B.M. Rumyantsev, S.B. Bibikov, A.V. Bychkova, V.G. Leontiev, V.I. Berendyaev, O.N. Sorokina, A.L. Kovarskii, Electric conductivity of polymer films filled with magnetic nanoparticles, Russian Journal of Physical Chemistry A. 90 (2016) 2426–2433. doi:10.1134/S0036024416120244.

[44] H.Q. Zhang, Y. Jin, Y. Qiu, The optical and electrical characteristics of PMMA film prepared by spin coating method, IOP Conference Series: Materials Science and Engineering. 87 (2015) 012032. doi:10.1088/1757-899X/87/1/012032.

[45] A.R. Blythe, Electrical resistivity measurements of polymer materials, Polymer Testing. 4 (1984) 195–209. doi:10.1016/0142-9418(84)90012-6.

[46] R. Farahmand, B. Sohrabi, A. Ghaffarinejad, M.R. Zamani Meymian, Synergistic effect of molybdenum coating and SDS surfactant on corrosion inhibition of mild steel in presence of 3.5% NaCl, Corrosion Science. 136 (2018) 393–401. doi:10.1016/j.corsci.2018.03.030.

[47] S.M. Rezaei Niya, M. Hoorfar, On a possible physical origin of the constant phase element, Electrochimica Acta. 188 (2016) 98–102. doi:10.1016/j.electacta.2015.11.142.

[48] S.C. Chung, J.R. Cheng, S.D. Chiou, H.C. Shih, EIS behavior of anodized zinc in chloride environments, Corrosion Science. 42 (2000) 1249–1268. doi:10.1016/S0010-938X(99)00129-8.

[49] F. Yang, H. Kang, E. Guo, R. Li, Z. Chen, Y. Zeng, T. Wang, The role of nickel in mechanical performance and corrosion behaviour of nickel-aluminium bronze in 3.5 wt.% NaCl solution, Corrosion Science. 139 (2018) 333–345. doi:10.1016/j.corsci.2018.05.012.

[50] G. Song, A. Atrens, M. Dargusch, In~uence of microstructure on the corrosion of diecast AZ80D, Corrosion Science. (n.d.) 25.

[51] J. Lee, D. Berman, Inhibitor or promoter: Insights on the corrosion evolution in a graphene protected surface, Carbon. 126 (2018) 225–231. doi:10.1016/j.carbon.2017.10.022.

[52] A. Bahramian, M. Eyraud, F. Vacandio, P. Knauth, Improving the corrosion properties of amorphous Ni-P thin films using different additives, Surface and Coatings Technology. 345 (2018) 40–52. doi:10.1016/j.surfcoat.2018.03.075.

[53] T. Pojtanabuntoeng, B. Kinsella, H. Ehsani, J. McKechnie, Assessment of corrosion control by pH neutralisation in the presence of glycol at low temperature, Corrosion Science. 126 (2017) 94–103. doi:10.1016/j.corsci.2017.06.018.

[54] G. Liu, Z. Huang, L. Wang, W. Sun, S. Wang, X. Deng, Effects of Ce4+ on the structure and corrosion resistance of electroless deposited Ni–Cu–P coating, Surface and Coatings Technology. 222 (2013) 25–30. doi:10.1016/j.surfcoat.2013.01.053.

[55] W. Xu, X. Lu, B. Zhang, C. Liu, S. Lv, S. Yang, X. Qu, Effects of Porosity on Mechanical Properties and Corrosion Resistances of PM-Fabricated Porous Ti-10Mo Alloy, Metals. 8 (2018) 188. doi:10.3390/met8030188.

[56] J. Creus, H. Mazille, H. Idrissi, Porosity evaluation of protective coatings onto steel, through electrochemical techniques, Surface and Coatings Technology. 130 (2000) 224–232. doi:10.1016/S0257-8972(99)00659-3.

[57] M.D. Vedenyapina, V.V. Kuznetsov, D.I. Rodikova, N.N. Makhova, A.A. Vedenyapin, Anodic corrosion of gold in solutions of diaminoalkanes, Mendeleev Communications. 28 (2018) 181–183. doi:10.1016/j.mencom.2018.03.024.

[58] G.S. Frankel, Pitting Corrosion of Metals, Journal of The Electrochemical Society. 145 (1998) 2186. doi:10.1149/1.1838615.

Tables

Table 1. Fitted values of C0 using the EC presented in Figure 7a

R_s (Ω.cm^2)	CPE$_{dl}$		R_{ct} (kΩ.cm^2)	CPE$_p$		R_p (kΩ.cm^2)
	Y° (μF.cm^{-2}.s^{n-1})	n		Y° (μF.cm^{-2}.s^{n-1})	n	
5.1±0.2	2.0±0.5	0.93±0.01	96±5	8.8±0.5	0.52±0.06	6±2

Table 2. Fitted values of PMMA modified samples using the EC presented in Figure 7b

Sample	R_s (Ω.cm^2)	CPE$_t$		R_t (kΩ.cm^2)
		Y° (μF.cm^{-2}.s^{n-1})	n	
C5	5.3 ± 0.8	24 ± 7	0.88 ± 0.02	150 ± 23
C10	6.0 ± 1.7	16 ± 4	0.87 ± 0.03	274± 24
C15	5.6 ± 0.1	21 ± 3	0.87 ± 0.02	161± 34
C25	5.9 ± 1.5	20 ± 4	0.86 ± 0.03	88± 15
C50	5.7 ± 0.9	39 ± 16	0.86 ± 0.03	25± 6
C100	6.0 ± 1.0	32 ± 6	0.83 ± 0.04	13± 5

Table 3. Corrosion current density, corrosion potential, anodic and cathodic slopes, and polarization resistance of Ni-P barrier layer and C0-C100

Sample	i_{corr} (μA.cm^{-2})	E_{corr} (mV) vs. Ag/AgCl	Average Tafel slope (mV. dec^{-1})		R_p (kΩ.cm^2)
			β_a	β_c	
Ni-P barrier layer	6.68 ± 0.78	-202 ± 7	137 ± 10	147 ± 14	5 ± 1
C0	0.50 ± 0.10	-110 ± 7	58 ± 5	196 ± 13	40 ± 8
C5	0.18 ± 0.02	-14 ± 23	149 ± 26	99 ± 5	148 ± 24
C10	0.08 ± 0.01	-36 ± 3	151 ± 9	102 ± 21	339 ± 92
C15	0.15 ± 0.04	4 ± 11	114 ± 39	114 ± 3	168± 28
C25	0.24 ± 0.10	-16 ± 20	128 ± 31	108 ± 4	116 ± 35
C50	1.93 ± 0.73	-33 ± 13	187 ± 40	135 ± 4	20 ± 8
C100	2.68 ± 1.92	-75 ± 13	199 ± 76	158 ± 42	17±8

Figures
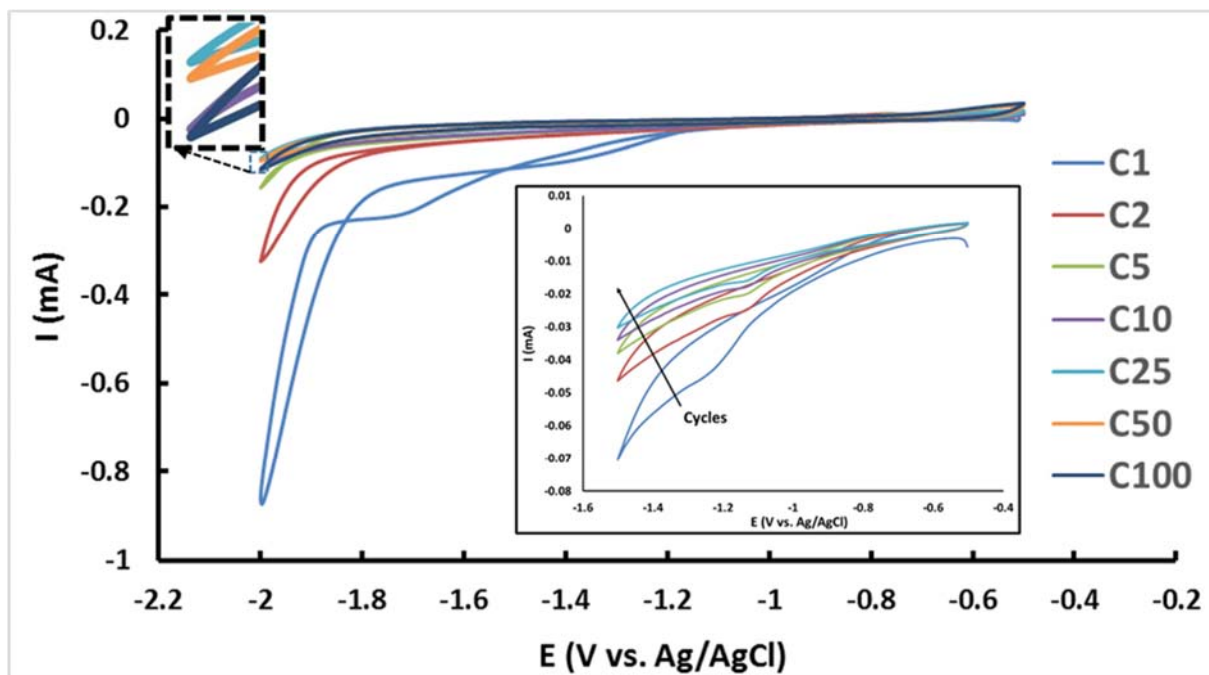
Figure 1. CV curves of cathodic electropolymerization of MMA on Cu/Ni-P/Au electrical contacts from 0.1 M KNO₃ DMSO solution with a scan rate of 20 mV.s⁻¹.
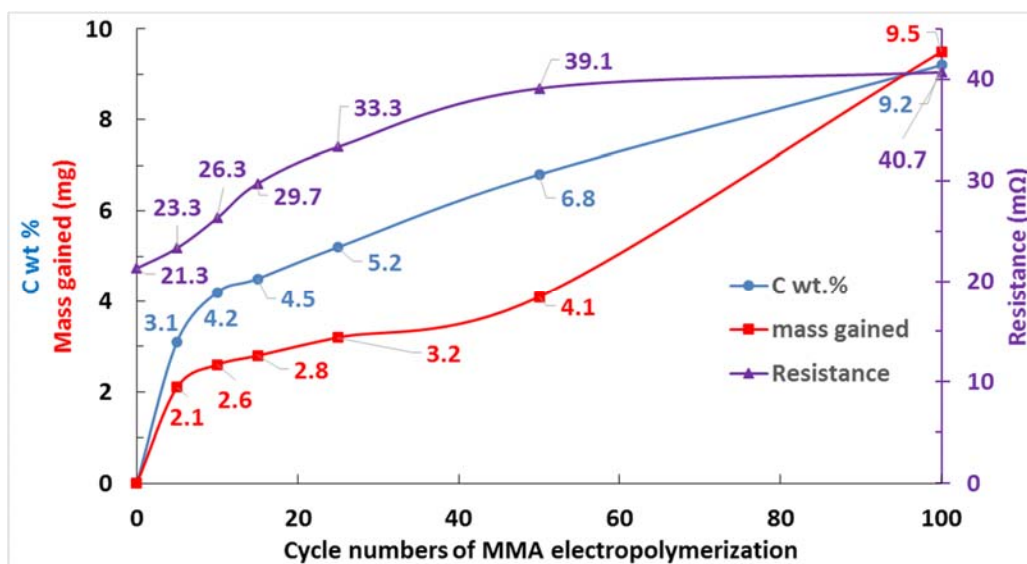
Figure 2. Mass gain, C content, and resistance as a function of electropolymerization cycle number.

17
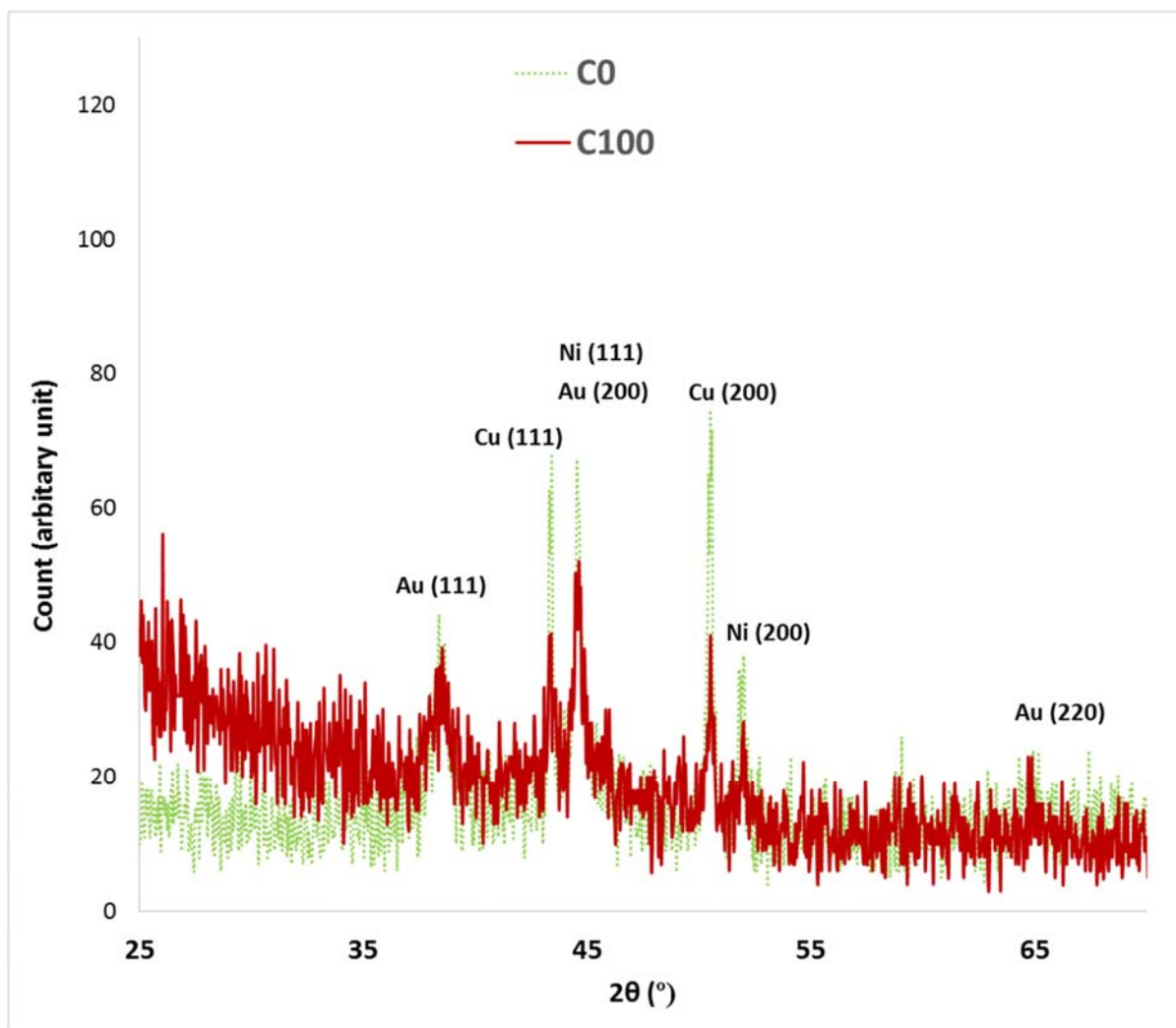
Figure 3. Grazing incidence XRD patterns of C0 and C100.
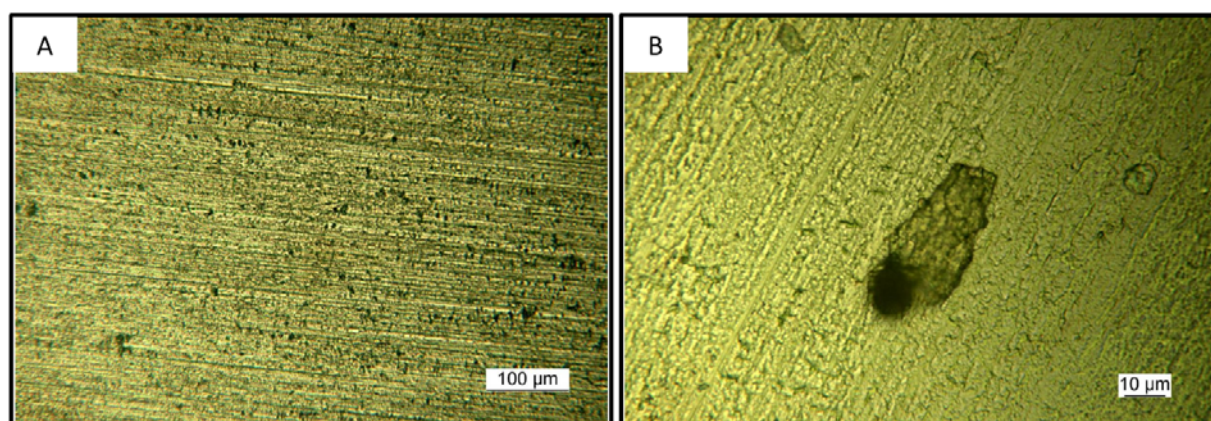
Figure 4. Optical micrograph of C0 at low (a) and high (b) magnifications.
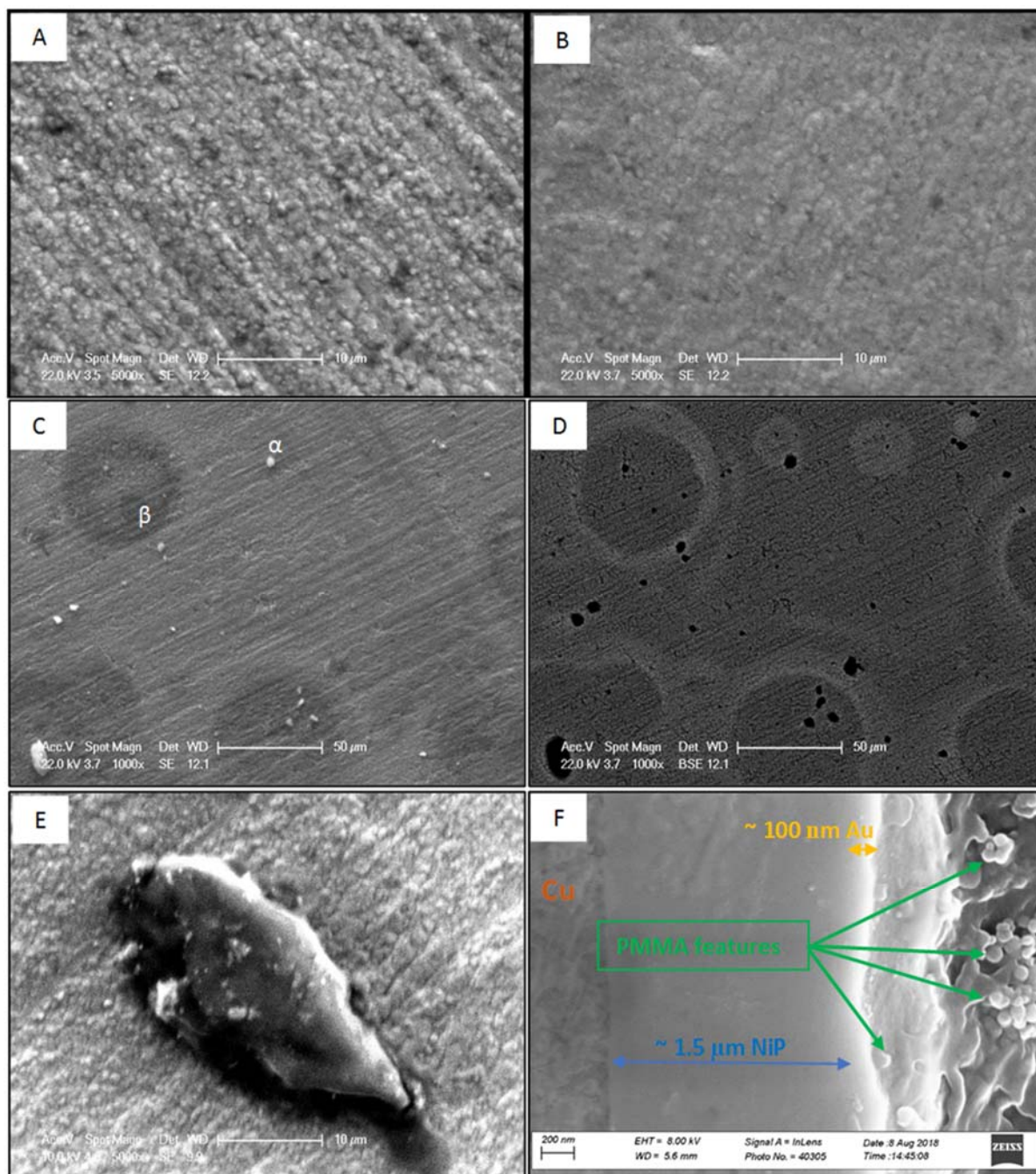
Figure 5. (a) SE SEM image of C0, (b) SE SEM image of C100, (c) SE SEM image of C100, (d) BSE SEM image of C100, (e) SE SEM image of C100 (10kV electron beam power), and (f) cross-section BSE SEM image of C100 .
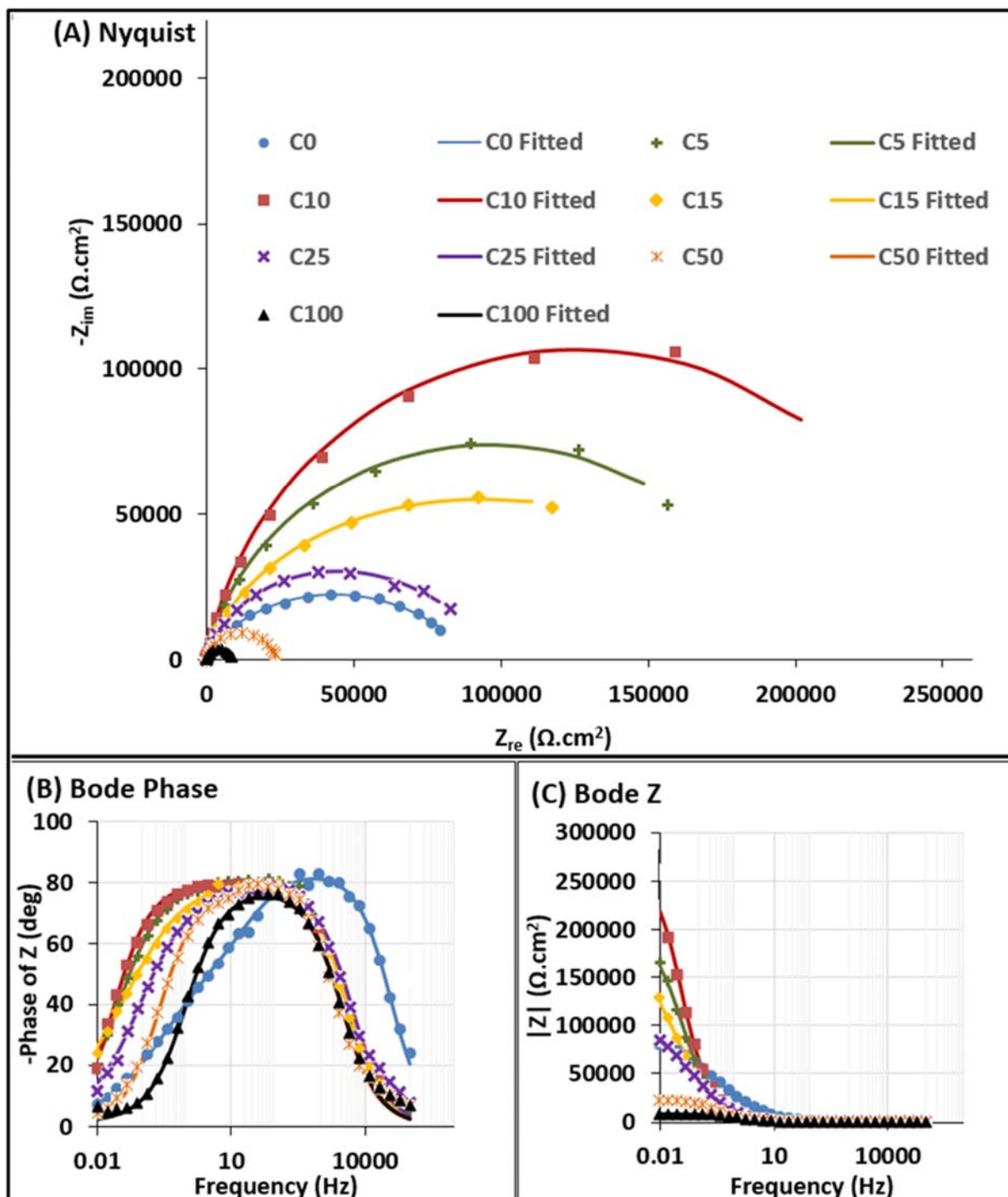
Figure 6. (a) Nyquist, (b) Bode Phase, and (c) Bode modulus curves of C0-C100 after one hour immersion in 3% NaCl solution.
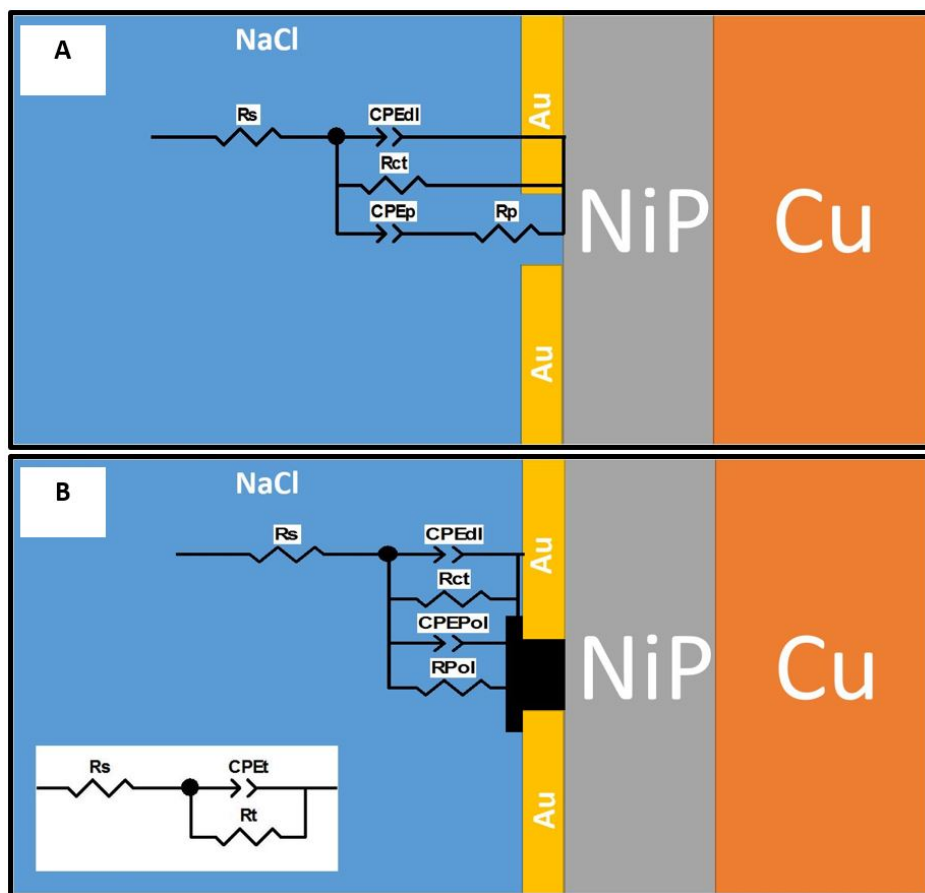
Figure 7. Proposed equivalent circuits to fit the EIS data of (a) C0, and (b) PMMA modified samples (C5-C100).
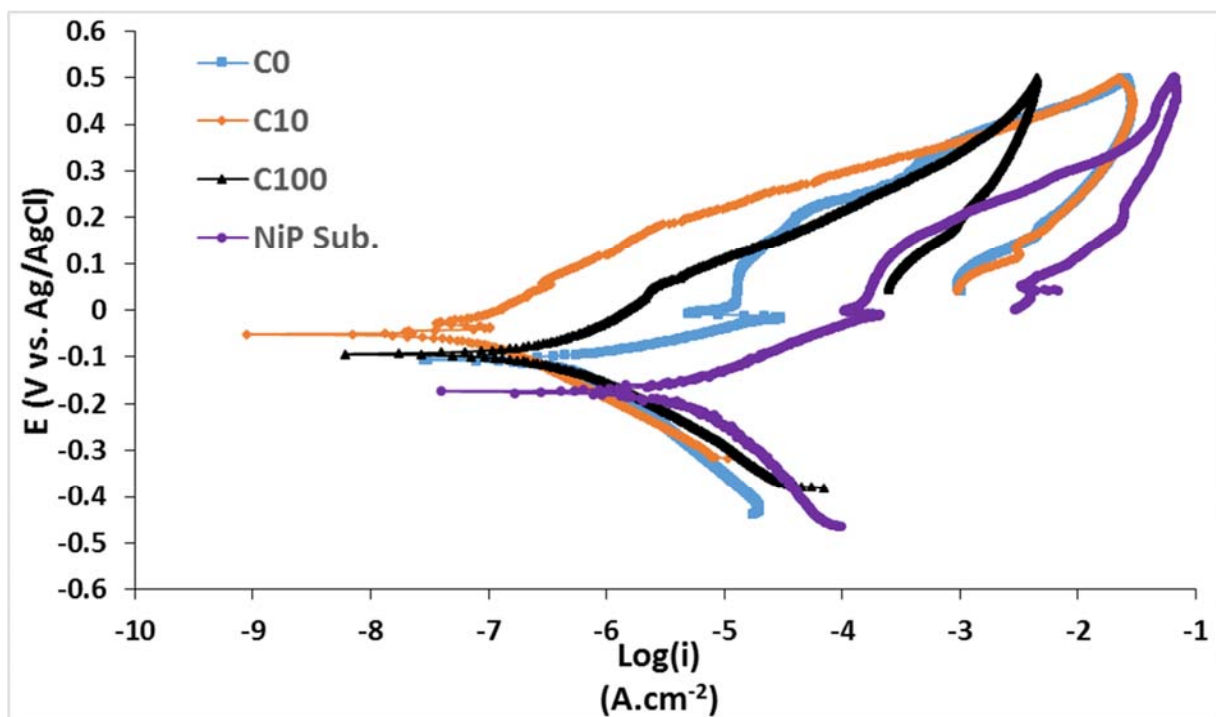
Figure 8. CP curves of C0, C10, C100, and the Ni-P substrate after one hour immersion in 3% NaCl solution.
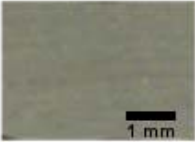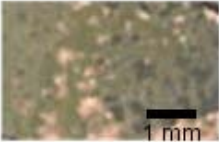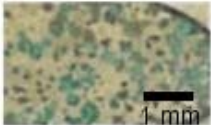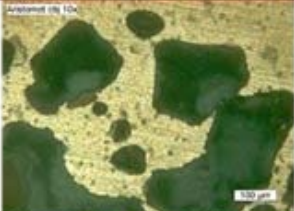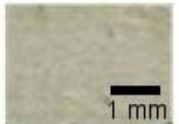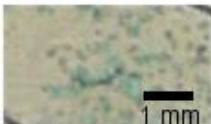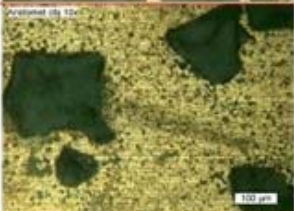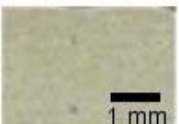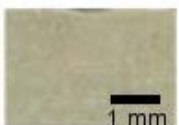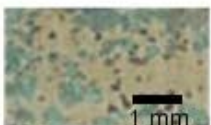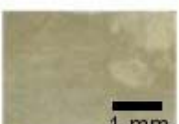
Modification with MMA	Before Corrosion	After Corrosion	
0 cycle			
5 Cycles			
10 cycles			
15 Cycles			
25 cycles			
50 cycles			
100 cycles			

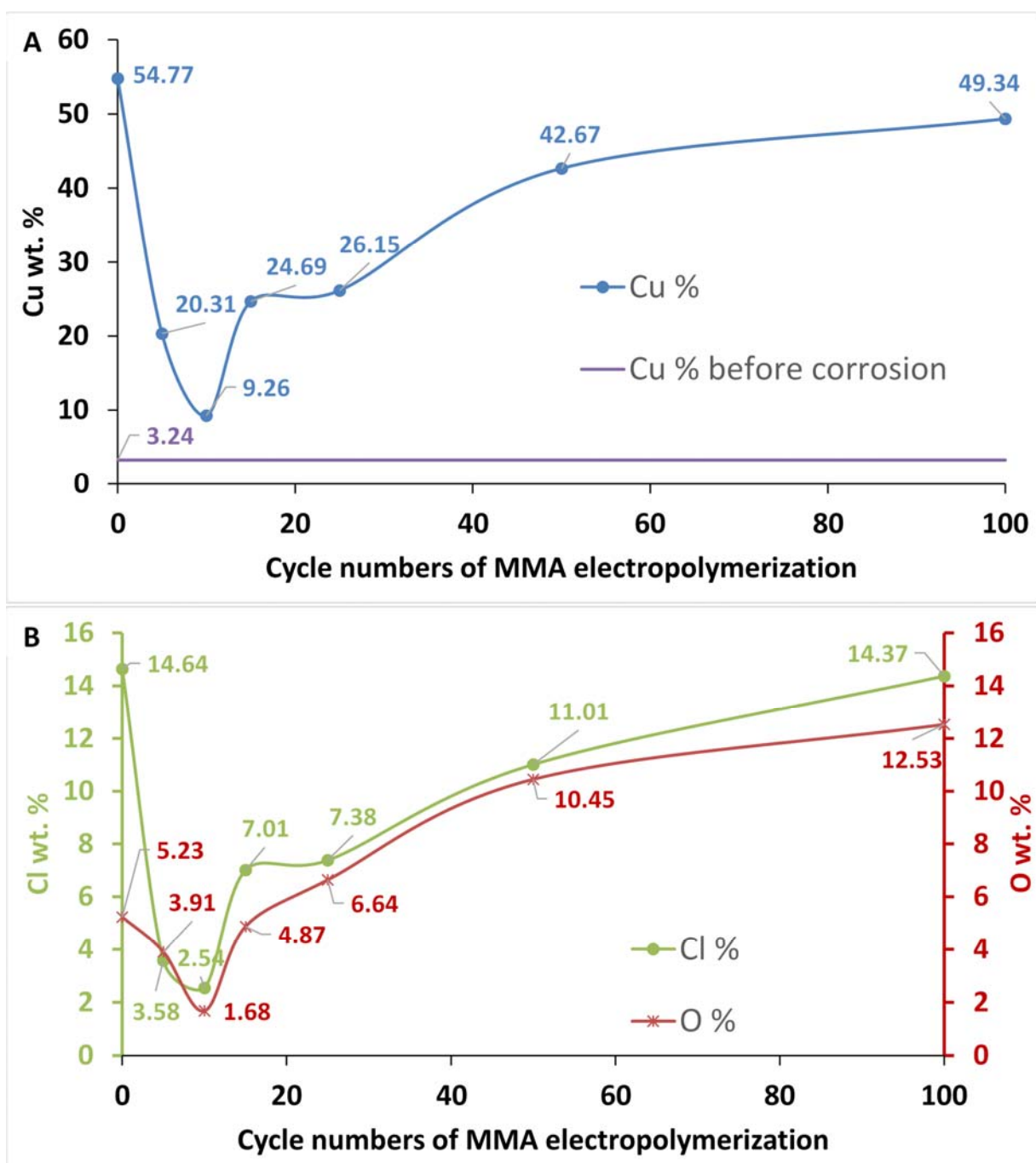*Figure 9. Surface of the samples before and after electrochemical corrosion tests.*

23

 Figure 10. (a) Cu wt.%, and (b) Cl wt.% and O wt.% of samples after the corrosion tests as a function of the electropolymerization cycle number.
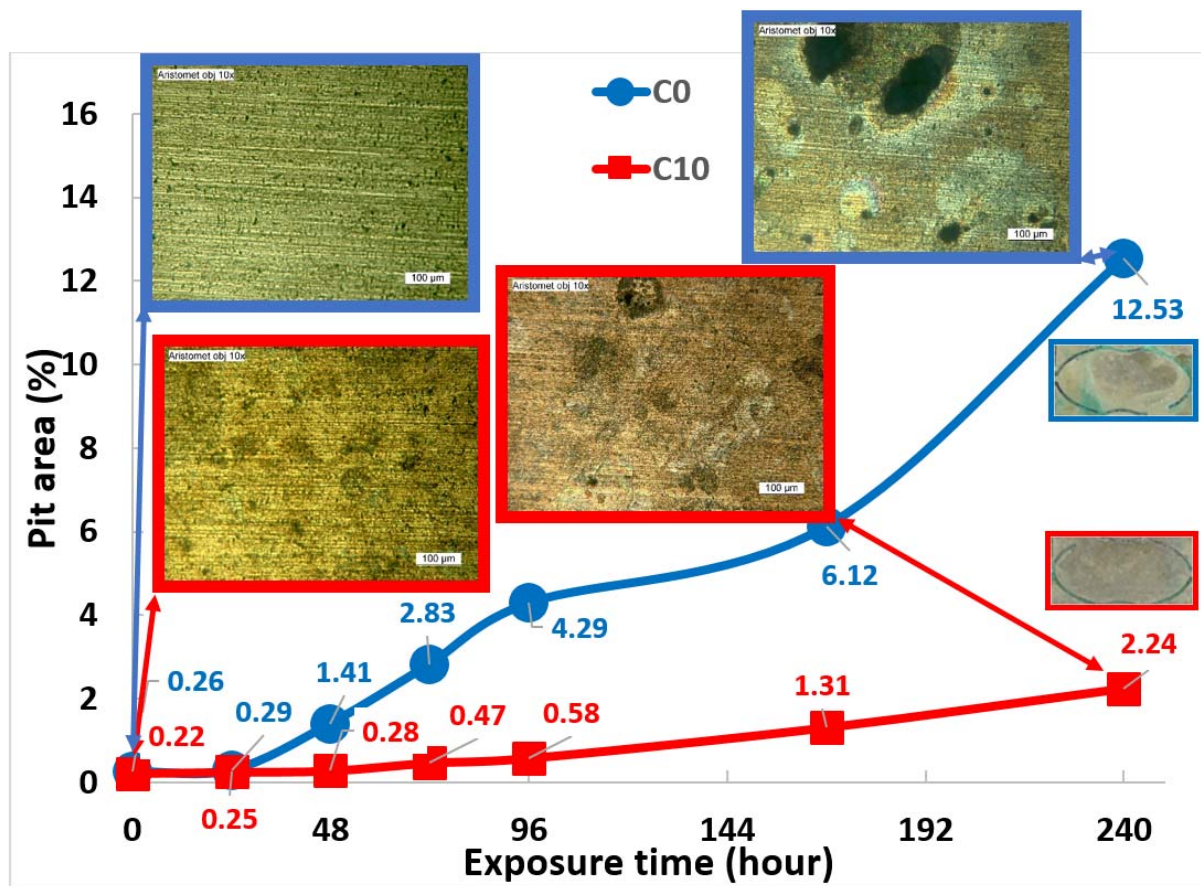
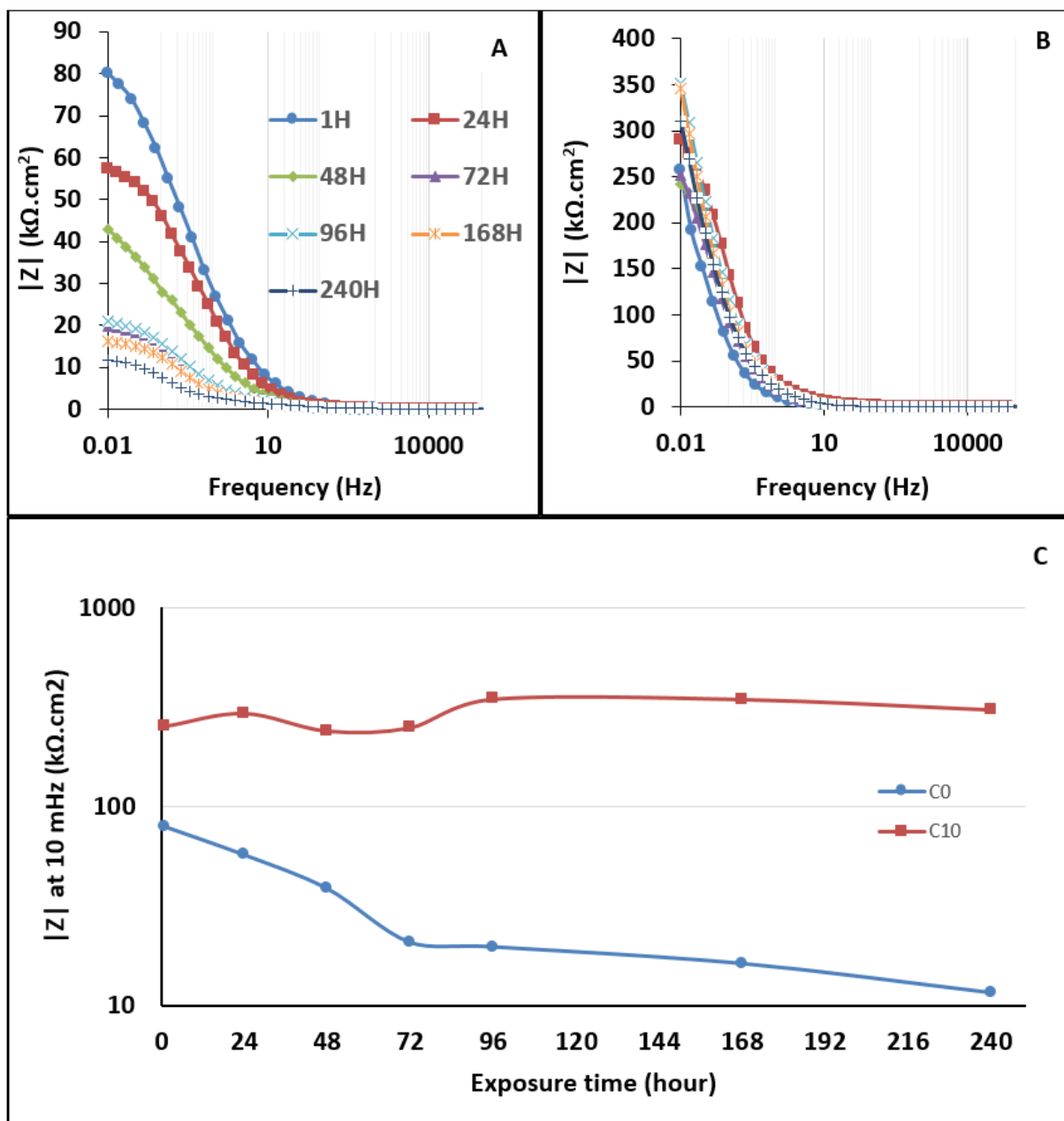*Figure 11. Pit area of C0 and C10 during 240 hours of salt spray test.*

Figure 12. Bode Z plots of (a) C0 and (b) C10 and (c) their |Z| values at 10 mHz during 240 hours immersion in 3% NaCl solution.